ADVANCED FUNCTIONAL MATERIALS

Supporting Information

for *Adv. Funct. Mater.,* DOI: 10.1002/adfm.201603230

High Strength Conductive Composites with Plasmonic Nanoparticles Aligned on Aramid Nanofibers

*Jing Lyu, Xinzhi Wang, Lehao Liu, Yoonseob Kim, Ekembu K. Tanyi, Hang Chi, Wenchun Feng, Lizhi Xu, Tiehu Li, Mikhail A. Noginov, Ctirad Uher, Mark D. Hammig, and Nicholas A. Kotov**

Supplementary Information

High Strength Conductive Composites with Plasmonic Nanoparticles Aligned on Aramid Nanofibers

Jing Lyu[1,2,3], Xinzhi Wang[1,2,4], Lehao Liu[1,2,3], Yoonseob Kim[1,2], Ekembu K. Tanyi[5], Hang Chi[6], Wenchun Feng[1,2], Lizhi Xu[1,2], Tiehu Li[3], Mikhail A. Noginov[5], Ctirad Uher[6], Mark D. Hammig[7], Nicholas A. Kotov[1,2,8,9,10] *

[1] Department of Chemical Engineering, University of Michigan, Ann Arbor, MI 48109, USA;
[2] Biointerfaces Institute, University of Michigan, Ann Arbor, MI 48109, USA;
[3] School of Materials Science and Engineering, Northwestern Polytechnical University, Xi'an 710072, P. R. China;
[4]School of Energy Science and Engineering, Harbin Institute of Technology, Harbin 150001, P. R. China;
[5]Center for Materials Research, Norfolk State University, Norfolk, VA 23504, USA;
[6] Department of Physics, University of Michigan, Ann Arbor, MI 48109, USA;
[7] Department of Nuclear Engineering and Radiological Sciences, University of Michigan, Ann Arbor, MI 48109, USA;
[8] Department of Materials Science and Engineering, University of Michigan, Ann Arbor, MI 48109, USA;
[9] Department of Biomedical Engineering, University of Michigan, Ann Arbor, MI 48109, USA;
[10] Michigan Center for Integrative Research in Critical Care, 2800 Plymouth Road, Ann Arbor, MI 48109, USA.

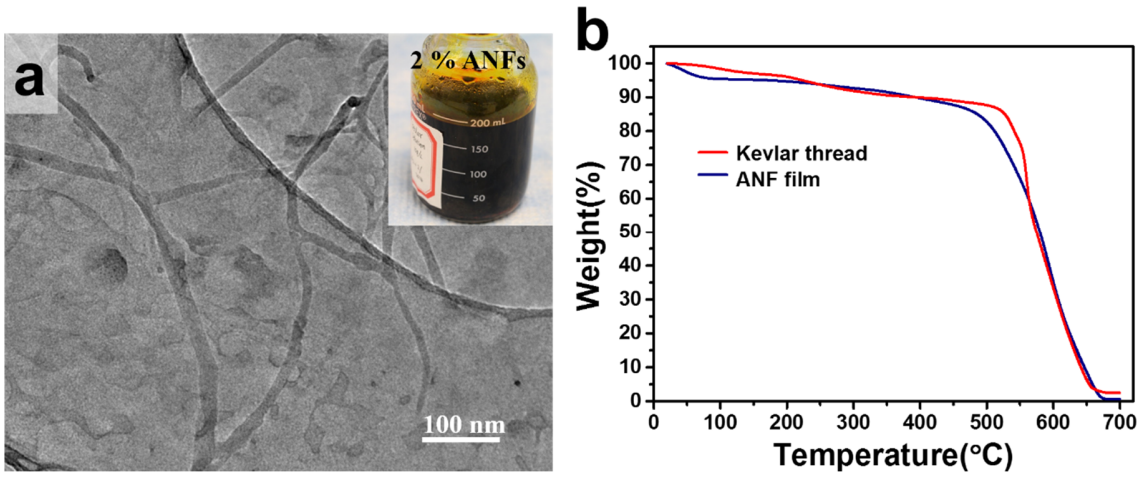

Figure S1. a, TEM image of ANFs. The inset is the photograph of 2% ANFs solution. b, Thermal gravimetric analysis (TGA) of Kevlar threads and ANF films.

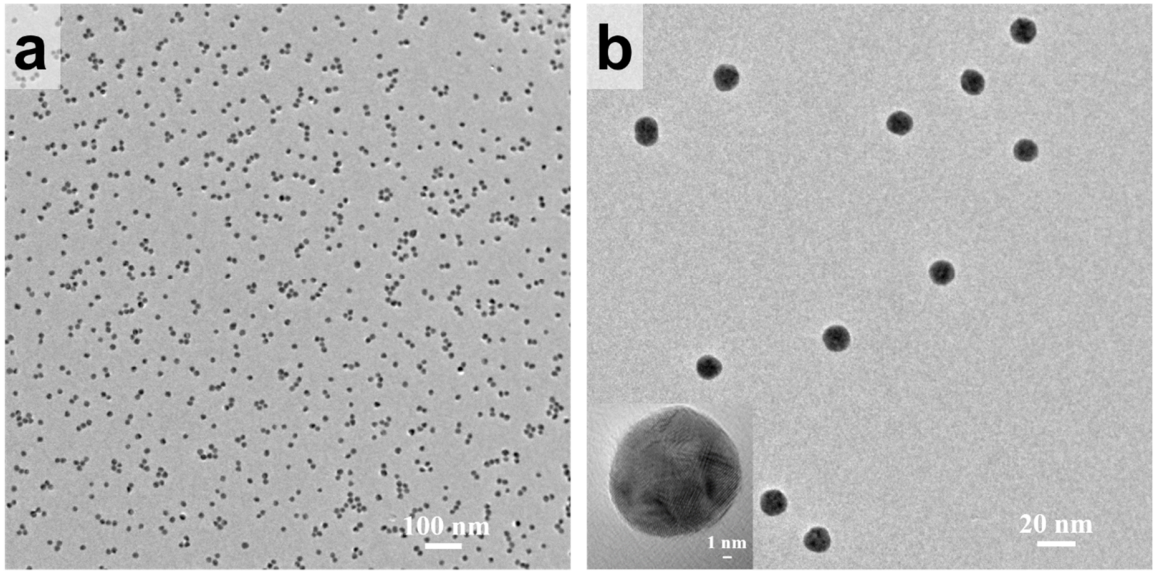

Figure S2. a, b, TEM images of gold nanoparticles.

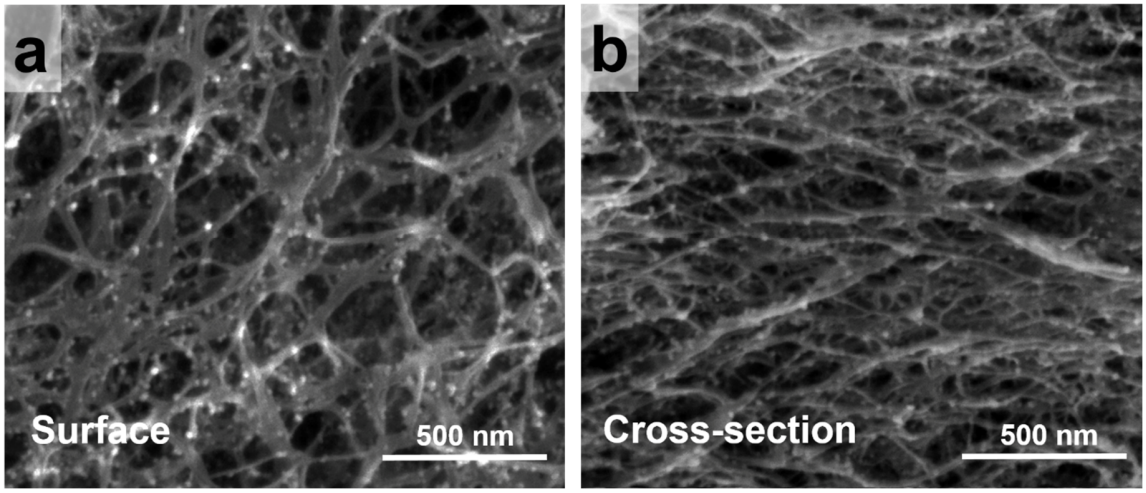

Figure S3. SEM images of Au-ANF films synthesized by immersing films in concentrated Au NPs solution. a, Surface SEM image. b, Cross-section of the film.

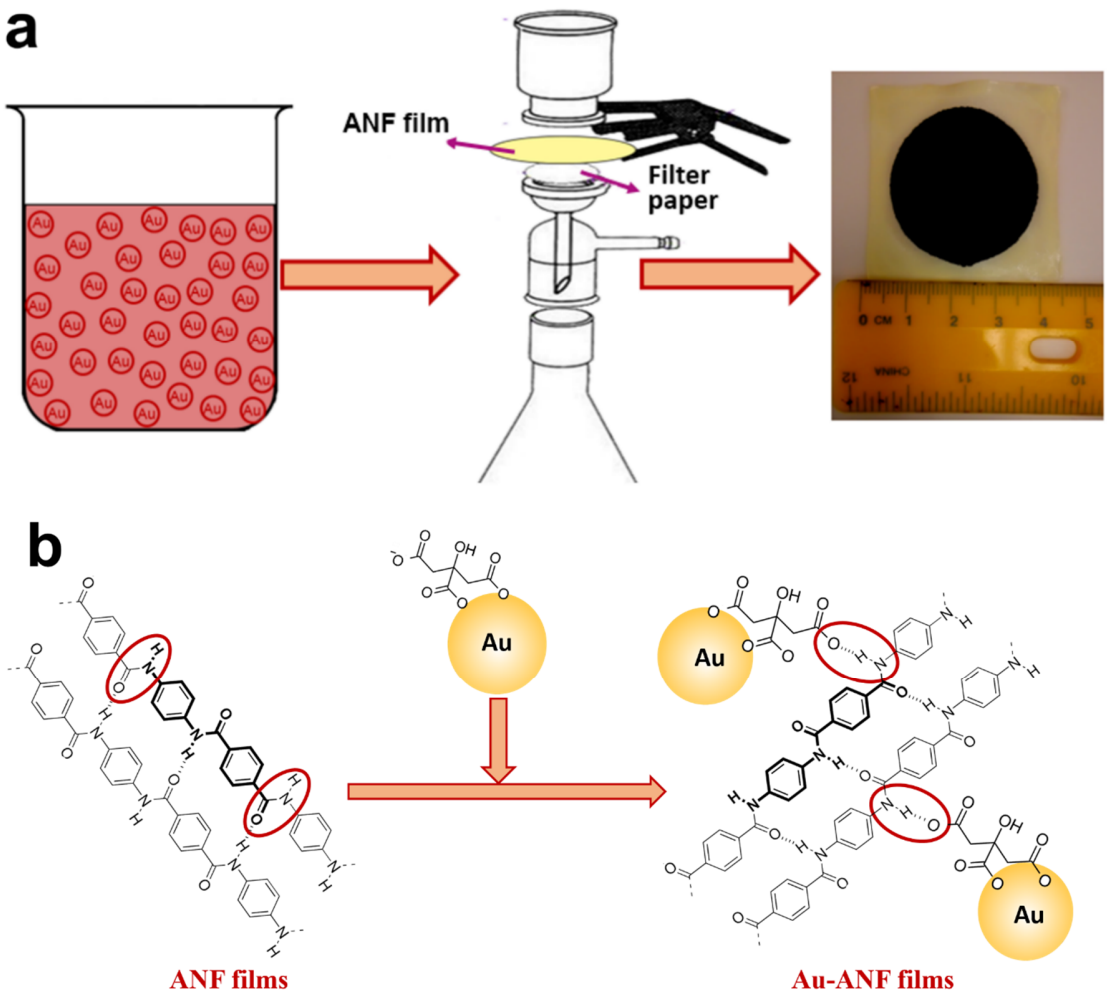

Figure S4. a, Schematic diagram of vacuum filtration to incorporate Au NPs into ANF films. b, Schematic diagram of the Au NPs adsorption on ANFs.

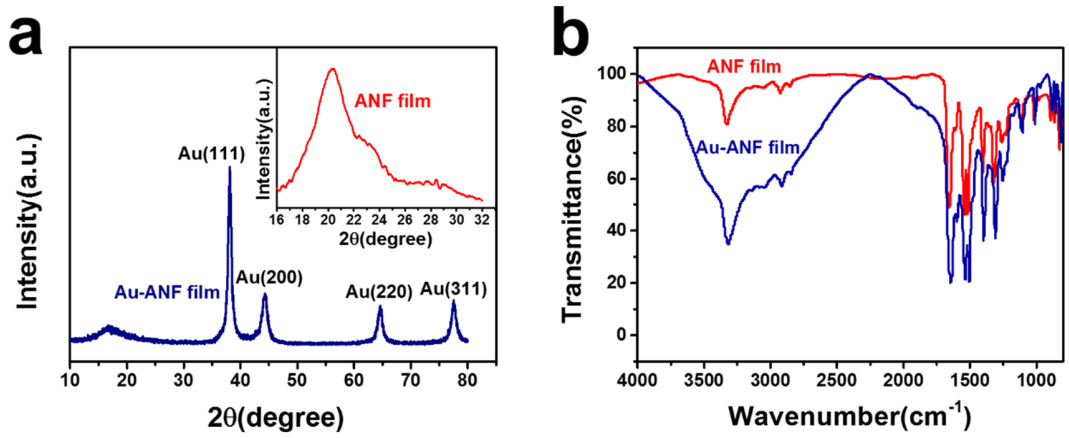

Figure S5. a, XRD pattern of Au-ANF films. Insert is the XRD pattern of ANF films. b, FT-IR spectra of ANF films and Au-ANF films.

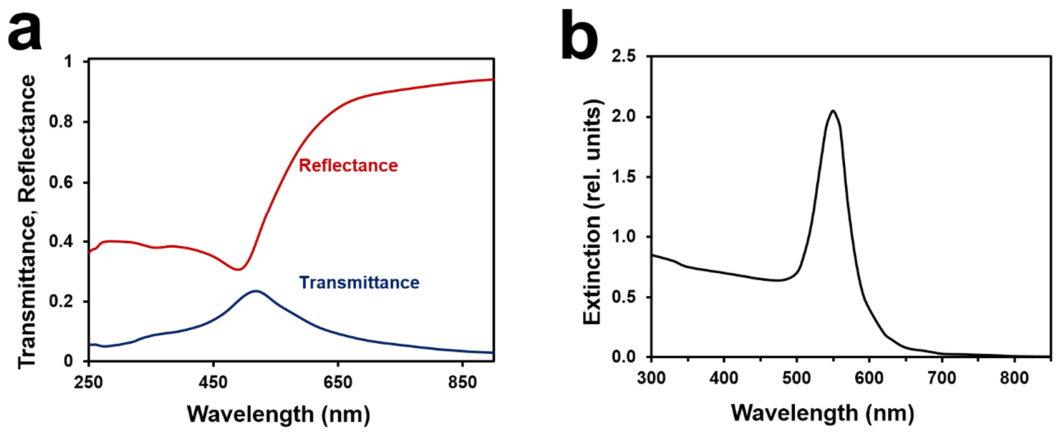

Figure S6. a, Reflectance and transmittance spectra of 35 nm Au film.[1,2,3] b, Extinction cross section spectrum of 13 nm Au NP described as nanospheres embedded in the dielectric medium with the refractive index n=1.7.[3,4]

Two characteristic optical responses of gold include (i) the onset of metallic reflectivity of bulk Au (0.55 μm), accompanied by the moderate enhancement of transmittance in thin Au films, Figure S7. a, and (ii) the band in the absorption and scattering spectra of Au NPs (≈0.55 μm, depending on the refractive index of surrounding medium), originating from localized surface plasmon (SP) resonances, Figure S7. b. Both phenomena have been observed in the reflectance and transmittance studies described in Figures S7 and S8.

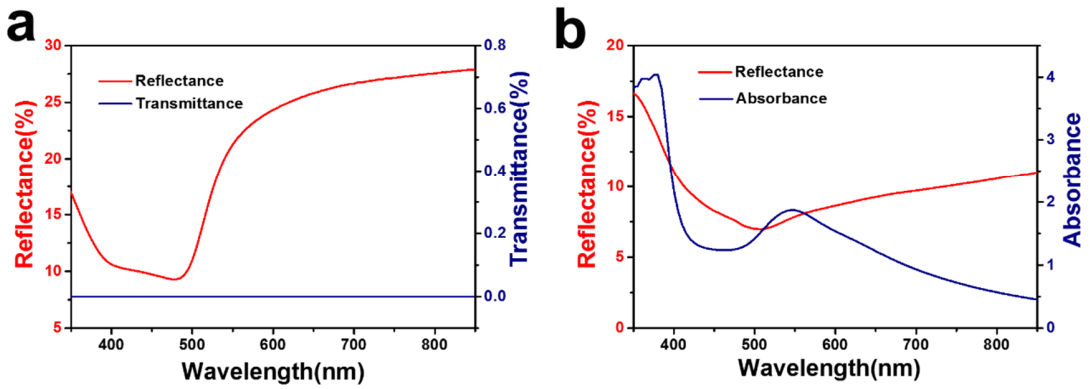

Figure S7. a, Reflectance and transmittance spectra of the Au-ANF films with 15.7 vol. % Au concentration. b, Reflectance and absorbance spectra of the Au-ANF films with 3.4 vol. % Au concentration.

The film thickness was ~2 μm. All films have been stretched over empty rectangular frames and did not have any supporting (and reflecting) background substrate. In the transmittance measurements, the samples were mounted on the front port of the integrating sphere, and in the reflectance measurements, they were mounted on the back of the sphere (at 8 degrees incidence angle). The reflected light, which had large diffuse component, was detected by the photomultiplier tube (PMT) installed in the bottom of the integrating sphere. The standard white diffuse reflector (Labsphere Inc. NH, USA) was used as 100% reference.

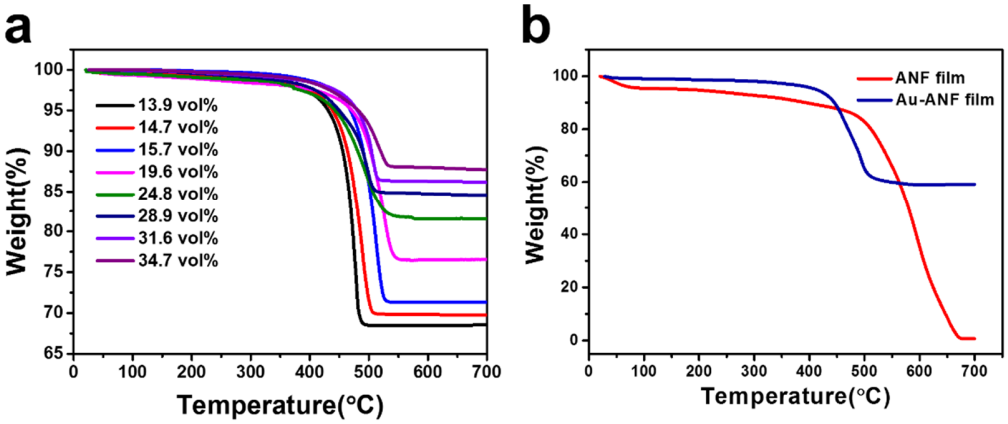

Figure S8. a, TGA of Au-ANF films with different Au content. b, Thermal gravimetric analysis (TGA) of ANF films and Au-ANF films.

The Au-ANF films containing 13.9 vol%, 14.7 vol%, 15.7 vol%, 19.6 vol%, 24.8 vol%, 28.9 vol%, 31.6 vol% and 34.7 vol% of Au NPs consumed 180 mL, 190 mL, 200 mL, 250 mL, 350 mL, 450 mL, 550 mL, and 650 mL of Au NPs solution, respectively.

The thermal stability of Au-ANF films decrease obviously comparing with pure ANF films. This may be explained through the higher heat capacity and thermal conductivity of Au NPs, which will cause it to preferably absorb the heat and quickly reach a higher temperature than the surrounding matrix (through the percolation pathways). This will cause degradation of ANF films at lower temperatures.

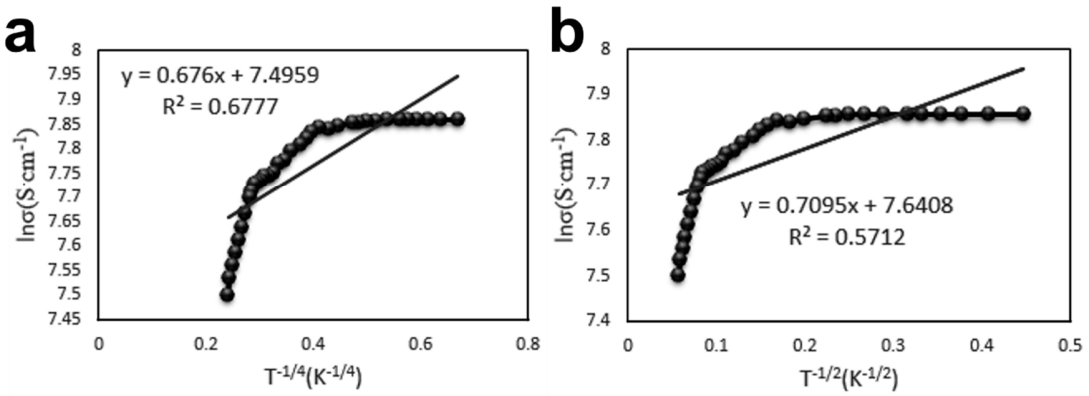

Figure S9. a, b, Natural logarithm of the conductivity σ *vs* $T^{-1/4}$ and $T^{-1/2}$ from data points of supercritical dried Au-ANF films (Figure 4c) according variable-range hopping and tunneling mechanisms equations, respectively.

In a variable-range hopping conduction process, the conductivity σ_H can be expressed as follow[5]

$$\sigma_H = \sigma_0 \cdot \exp[-(A/T)^{1/4}] \quad (1)$$

and in a tunneling mechanism, the conductivity σ_T is given by[6]

$$\sigma_T = \sigma_0 \cdot \exp[-(B/T)^{1/2}] \quad (2)$$

where σ_0 can be considered as the limiting value of conductivity at infinite temperature. The common feature of the plots is that the natural logarithm of the conductivity does not show a linear dependence on $T^{-1/4}$ or $T^{-1/2}$, which is indicative of variable-range hopping or tunneling conduction, respectively.

Table S1. The average crystal size of Au NPs in supercriticaly dried Au-ANF films and after thermal annealing at different temperatures

Temperature	RT	200 °C	250 °C	300 °C	350 °C	400 °C
Intensity	981	1066	1132	1192	1218	2064
FWHM	0.749	0.578	0.553	0.500	0.444	0.422
Crystallite (nm)	11.7	15.2	15.9	17.6	19.8	20.8

The average crystal size was determined by Scherrer equation: $D = \frac{k \cdot \lambda}{\beta \cdot cos\theta}$, where λ is the wavelength of the radiation (1.5406 Å for Cu Kα radiation), k is a constant equal to 0.94, β is the full width at half maximum (FWHM) and θ is the Bragg angle. The (1 1 1) plane of Au NPs in the XRD pattern of Au-ANF films was chosen to calculate the average crystal size.

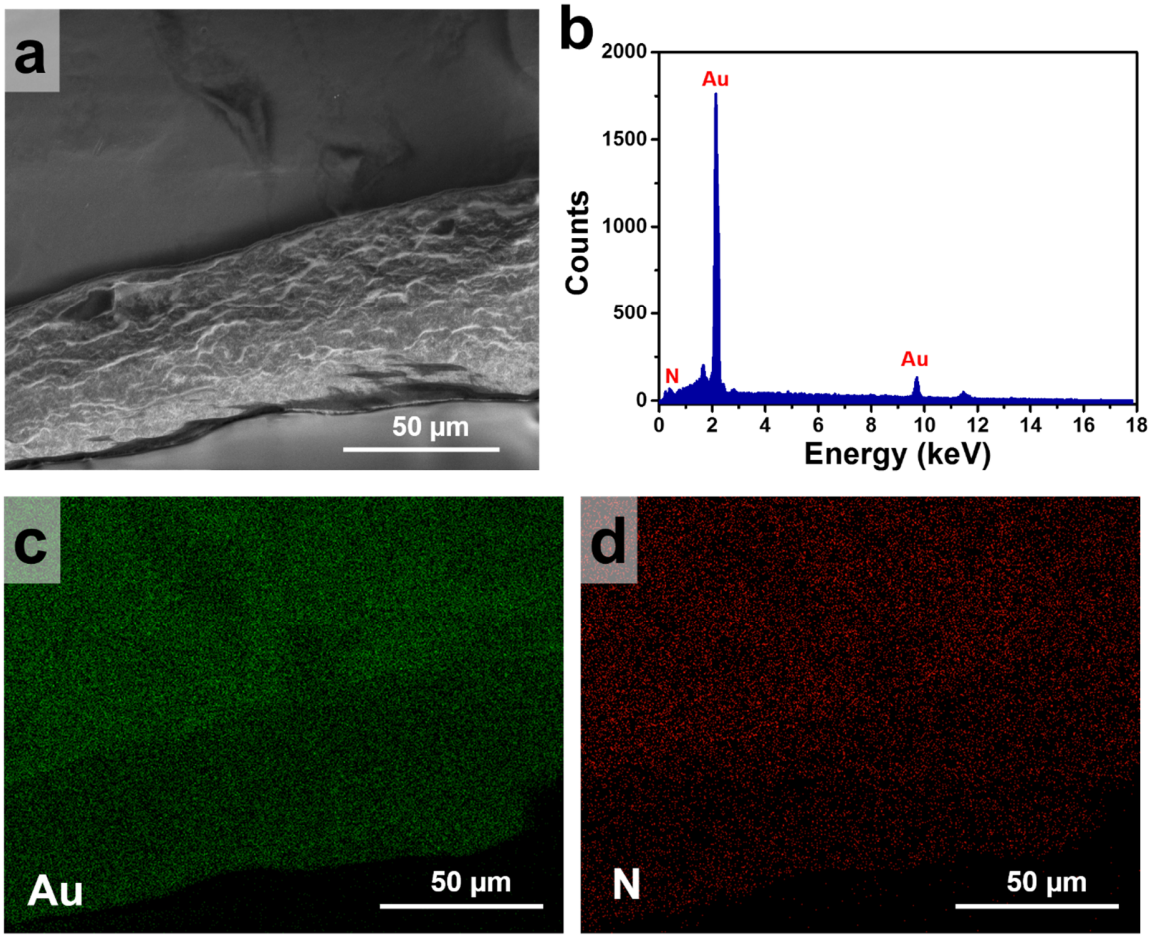

Figure S10. a-d, SEM image of Au-ANF films and the corresponding EDS mapping.

REFERENCES

(1) Ishii, S.; Chettiar, U. K.; Ni X. J.; Kildishev, A. V. PhotonicsRT: Wave Propagation in Multilayer Structures **2014**, https://nanohub.org/resources/photonicsrt. (DOI: 10.4231/D3MK6588C).

(2) Ni X. J.; Liu Z. T.; Kildishev, A. V. PhotonicsDB: Optical Constants. **2015**, https://nanohub.org/resources/PhotonicsDB. (DOI: 10.4231/D35H7BV58).

(3) Johnson, P. B.; Christry, R. W. Optical Constants of the Noble Metals. *Phys. Rev. B* **1972**, *6*, 4370–4379.

(4) http://www.lightscattering.de/MieCalc/eindex.html

(5) Psarras, G. C. Hopping Conductivity in Polymer Matrix-Metal Particles Composites. *Compos. Part A Appl. Sci. Manuf.* **2006**, *37*, 1545–1553.

(6) Ma, Y. G.; Liu, H. J.; Ong, C. K. Electron Transport Properties in CoAlO Composite Antidot Arrays. *Europhys. Lett.* **2007**, *76*, 1144–1150.